solution of the monodentate and chelated cations can differ by as much as 34 eu. It is largely coincidental if the entropy change for a chelation reaction is close to the ideal value. The same is true for the enthalpies of solution of the ligands. These can easily deviate from ideal by more than 4.8 kcal. (The enthalpies of solution of the coordinated cations probably differ also, but we are not in a position to estimate the amount.)

Registry No. $Cd(NH_3)_4^{2+}$, 18373-05-2; $Cd(MeNH_2)_4^{2+}$, 65516-97-4; $Cd(H_2O)_4^{2+}$, 15906-02-2; $Cu(NH_3)_4^{2+}$, 16828-95-8; $Cu(MeNH_2)_4^{2+}$, 30809-52-0; en, 107-15-3; pn, 78-90-0; eg, 107-21-1.

References and Notes

(1) F. M. Jones and E. M. Arnett, *Prog. Phys. Org. Chem.*, **11**, 263–322 (1974).
(2) A. E. Martell, *Adv. Chem. Ser.*, **No. 62**, 272–94 (1967).
(3) S. E. Rasmussen, *Acta Chem. Scand.*, **10**, 1279 (1956).
(4) D. Munro, *Chem. Brit.*, **13**, 100–105 (1977).
(5) R. T. Myers, *J. Chem. Educ.*, **53**, 17–19 (1976).
(6) W. D. Good and R. T. Moore, *J. Chem. Eng. Data*, **15**, 150 (1970).
(7) Unless indicated in the text, all thermodynamic data are taken from D. D. Wagman et al., *Natl. Bur. Stand., (U.S.), Tech. Note*, **No. 270** (1969), or from D. R. Stull, E. F. Westrum, and G. C. Sinke, "Chemical Thermodynamics of Organic Compounds", Wiley, New York, N.Y., 1969.
(8) J. M. Corkhill, J. F. Goodman, and J. R. Tate, *Trans. Faraday Soc.*, **65**, 1742 (1969).
(9) The scarcity of data is indeed unfortunate and is a real handicap to our understanding of this as well as other processes. For example, 1,2-ethanediamine, which may be considered one of the most important compounds in inorganic chemistry, has not had its entropy measured nor has the standard enthalpy and entropy of solution been measured. A concerted effort needs to be made to acquire basic thermodynamic data for common substances.
(10) G. Geiseler, *Naturwissenschaften*, **39**, 569 (1952).
(11) M. Lucas, *Bull. Soc. Chim. Fr.*, **64**, 1742 (1969).
(12) R. E. Powell and W. M. Latimer, *J. Chem. Phys.*, **19**, 1139 (1951).
(13) R. M. Smith and A. E. Martell, "Critical Stability Constants", Vol. 2, Amines, Plenum Press, New York, N.Y., 1975.
(14) N. S. Chhonkar, *Z. Phys. Chem. (Leipzig)*, **250**, 390–406 (1972).
(15) F. R.-Y. Shu, *Diss. Abstr. B*, **32**, 2571 (1971).

Contribution No. 2511 from the Central Research and Development Department, E. I. du Pont de Nemours and Company, Experimental Station, Wilmington, Delaware 19898

Ionic Conductivity in $Na_5YSi_4O_{12}$-Type Silicates

R. D. SHANNON,* B. E. TAYLOR, T. E. GIER, H.-Y. CHEN, and T. BERZINS

Received August 8, 1977

A new series of Na ion conductors of the type $Na_5MSi_4O_{12}$, where M = Fe, In, Sc, Y, and the rare earths Lu–Sm, has been prepared by hydrothermal and solid-state reactions. Na ion conductivities, measured with Na electrodes at $\sim 10^3$ Hz, are proportional to the size of M^{3+} and range from 2×10^{-3} $(\Omega\ cm)^{-1}$ for $Na_5ScSi_4O_{12}$ to 3×10^{-1} $(\Omega\ cm)^{-1}$ at 300 °C for $Na_5SmSi_4O_{12}$. This behavior is consistent with a structure consisting of $Si_{12}O_{36}$ rings stacked to form columns held apart by MO_6 octahedra. Immobile Na atoms are situated within the rings and mobile Na atoms between the columns. The size of the channels is dictated by the size of the MO_6 octahedra. $Na_5GdSi_4O_{12}$ and $Na_{5-x}Gd_{1-x}Zr_xSi_4O_{12}$, which can be sintered to 95% theoretical density and appear to be resistant to attack by Na, are probably the most practical materials for use as a solid electrolyte.

Introduction

The discovery of ionic conductivity in Na-β-Al_2O_3 has led to an intensive search for other conductive compositions.[1-7] The only oxide to show comparable Na ion conductivity has been $Na_3Zr_2PSi_2O_{12}$[8] (for $Na_3Zr_2PSi_2O_{12}$ $\sigma(300\ °C) \simeq 2 \times 10^{-1}$ $(\Omega\ cm)^{-1}$ and $E_a = 6.7$ kcal/mol[8] whereas for β-Al_2O_3 $\sigma(300\ °C) \simeq 2 \times 10^{-1}$ $(\Omega\ cm)^{-1}$ and $E_a = 3.8$ kcal/mol[9]).

$Na_5FeSi_4O_{12}$ was first discovered by Bowen, Schairer, and Willems[10] in their investigation of the Na_2O–Fe_2O_3–SiO_2 system. They prepared birefringent, hexagonal-prismatic crystals, but no x-ray data were reported. Hydrothermal synthesis of isotypic $Na_5YSi_4O_{12}$, $Na_5ScSi_4O_{12}$, and $Na_5ErSi_4O_{12}$ and the crystal structure of $Na_5YSi_4O_{12}$ was reported by Maksimov et al.[11-13] Because they could locate only 48/90 of the Na atoms in $Na_5YSi_4O_{12}$, we suspected that the remaining Na atoms might be mobile, making this compound a good Na ion conductor. Subsequent conductivity measurements showed $\sigma(200\ °C) = 4 \times 10^{-2}$ $(\Omega\ cm)^{-1}$ and $E_a = 7.1$ kcal/mol for $Na_5YSi_4O_{12}$. Further investigation showed that the Na rare earth silicates prepared by Maksimov hydrothermally could be made by solid-state reaction and that compounds with rare earth ions having even larger ionic radii than that of Y could be prepared.

In this paper we report ionic conductivities comparable to that of β-Al_2O_3 and $Na_3Zr_2PSi_2O_{12}$ in a series of compositions $Na_5MSi_4O_{12}$ where M = Fe, In, Sc, Y, and the rare earths Lu → Sm.

Experimental Section

Starting materials were reagent grade Na_2CO_3, $NaHCO_3$, SiO_2, GeO_2, ZrO_2, HfO_2, and rare earth oxides. In a typical preparation stoichiometric compositions were intimately mixed in an agate ball mill, heated in air to ~900–1050 °C in Pt crucibles for 16 h, quenched, ball milled again, reheated, and quenched.

Crystals of $Na_5YSi_4O_{12}$ were grown hydrothermally. A $^3/_8$ in. diameter gold tube, 6 in. long and sealed at one end, was charged with 4.26 g of $Na_2SiO_3 \cdot 9H_2O$, 1.20 g of NaOH pellets, and 0.11 g of Y_2O_3. After sealing, the tube was heated to 900 °C under 3000 atm of external hydrostatic pressure, cooled over 90 h to 400 °C, and then quenched. Removal of the flux with hot water left a residue of 0.36 g of 3–4 mm euhedral crystals of $Na_5YSi_4O_{12}$. Only a small range of Na/Si ratios is possible—if this ratio is too small, $Na_3YSi_3O_9$ is stable; if too large, $Na_3YSi_2O_7$ and $NaYSiO_4$ form.

X-ray patterns were obtained on a Hägg–Guinier camera using Cu $K\alpha_1$ radiation and a KCl internal standard ($a = 6.2931$ Å). Table I gives powder diffraction data for $Na_5FeSi_4O_{12}$ and $Na_5YSi_4O_{12}$; Table II gives cell dimensions of some of the silicates and germanates prepared in this study. A low-temperature x-ray diffractometer pattern of $Na_5YSi_4O_{12}$ (NYS) was taken at 9 K; no superstructure lines were observed.

DTA scans were made with a du Pont thermal analyzer. High-temperature x-ray patterns were obtained with a Nonius Guinier camera. The results of the DTA investigations are summarized in Table III. The Fe, Sc, In, Lu, and Er compositions show small unexplained exothermic peaks at about 500–600 °C. Most compositions show small unexplained endotherms at ~800 °C. $Na_5FeSi_4O_{12}$ melts at 815 °C, whereas most of the other compositions melt between 1100 and 1250 °C, probably incongruently. Quenching experiments on $Na_5YSi_4O_{12}$ (NYS) showed NYS at 1150 °C, NYS + $Na_3YSi_2O_7$ at 1200 °C, and $Na_3YSi_2O_7$ at 1250 °C. Similar experiments on $Na_5GdSi_4O_{12}$ (NGS) showed NGS at 1060 °C and NGS + a $Ca_3Al_2O_6$-like phase at 1080 °C.

High-temperature Guinier photographs were obtained to explain some of the DTA thermal events. The high-temperature run for $Na_5ScSi_4O_{12}$ was carried out under vacuum. At 500 °C, lines appeared from a phase similar to $Ca_3Al_2O_6$ (C_3A). Formation of this phase may be responsible for the 600 °C exotherm. From 500 to 815 °C, $Na_5ScSi_4O_{12}$ and the C_3A phase coexist. At 850 °C, both these phases disappear and a new unidentified phase with strong lines at 4.45, 4.15,

0020-1669/78/1317-0958$01.00/0

Table I. Powder Diffraction Data for $Na_5FeSi_4O_{12}$ and $Na_5YSi_4O_{12}$

	$Na_5FeSi_4O_{12}$				$Na_5YSi_4O_{12}$		
Index	d_{obs}	d_{calc}	I_o	Index	d_{obs}	d_{calc}	I_o
211	6.091	6.091	45	211	6.259	6.260	55
220	5.354	5.355	45	220	5.506	5.508	50
410	4.047	4.048	25	131	4.891	4.879	2
312	3.945	3.946	40	410	4.162	4.164	40
113	3.827	3.829	25	321	4.133	4.135	10
042	3.702	3.703	10	312	4.051	4.052	60
232	3.501	3.499	5	113	3.925	3.925	55
223	3.256	3.255	10	042	3.805	3.803	2
502	3.176	3.177	10	232	3.594	3.595	15
600	3.092	3.092	15	223	3.340	3.340	10
024	2.917	2.918	15	511	3.306	3.307	25
413	2.880	2.880	15	502	3.264	3.264	10
214	2.818	2.816	2	600	3.179	3.180	25
342	2.732	2.732	5	024	2.992	2.992	35
333	2.692	2.692	5	413	2.957	2.957	10
440	2.677	2.677	100	214	2.886	2.887	5
134	2.639	2.639	30	161	2.834	2.835	2
701	2.590	2.590	2	342	2.807	2.808	10
404	2.562	2.562	45	333	2.762	2.764	10
612		2.570		440	2.753	2.754	100
710	2.456	2.457	2	134	2.707	2.707	45
523	2.405	2.405	2	404	2.629	2.629	50
054	2.368	2.367	2	532	2.502	2.502	10
262		2.373		015		2.499	
244	2.310	2.311	2	523	2.471	2.471	15
811	2.139	2.138	5	262	2.439	2.439	5
550		2.142		205		2.437	
235	2.128	2.129	5	054	2.429	2.429	15
722		2.126		125	2.379	2.379	10
900	2.059	2.061	5	244		2.372	
731		2.057		271	2.291	2.292	15
182	2.048	2.047	5	811	2.199	2.199	2
006		2.050		550		2.203	
505		2.050		235	2.184	2.184	10
116	2.013	2.013	2	722		2.186	
425		2.013		731	2.116	2.116	15
642		2.011		900		2.120	
704	2.006	2.007	2	006	2.101	2.100	10
155	1.978	1.979	2	505		2.103	
372		1.976		182		2.105	
306	1.945	1.945	2	116	2.062	2.063	25
651	1.921	1.920	10	704		2.061	
740		1.923		425		2.066	
084	1.852	1.851	10	642		2.067	
912		1.854		155	2.029	2.030	2
615		1.856		372		2.032	
832	1.801	1.801	10	624		2.026	
535		1.803		306	1.994	1.994	5
075		1.803		651	1.975	1.975	25
814	1.774	1.773	10	740		1.978	
0102		1.776		084	1.901	1.901	35
336		1.777		615		1.905	
265		1.778		921	1.859	1.859	10
292	1.751	1.752	2	832	1.851	1.851	25
464		1.749		535		1.850	
107		1.749		075		1.850	

Table II. Cell Dimensions of Compounds Having the $Na_5YSi_4O_{12}$ Structure

Compd	*a*, Å	*c*, Å	*V*, Å^3
$Na_5FeSi_4O_{12}$	21.425 (2)	12.300 (2)	4889
$Na_5ScSi_4O_{12}$	21.672 (3)	12.437 (2)	5058
$Na_5InSi_4O_{12}$	21.725 (2)	12.460 (2)	5093
$Na_5LuSi_4O_{12}$	21.920 (2)	12.576 (2)	5233
$Na_5YbSi_4O_{12}$	21.940 (2)	12.567 (2)	5239
$Na_5TmSi_4O_{12}$	21.958 (3)	12.579 (2)	5252
$Na_5ErSi_4O_{12}$	21.989 (2)	12.610 (2)	5280
$Na_5HoSi_4O_{12}$	22.034 (2)	12.607 (2)	5301
$Na_5YSi_4O_{12}$	22.035 (1)	12.604 (1)	5300
$Na_5DySi_4O_{12}$	22.058 (2)	12.623 (3)	5319
$Na_5TbSi_4O_{12}$	22.083 (1)	12.627 (1)	5332
$Na_5GdSi_4O_{12}$	22.126 (5)	12.650 (4)	5363
$Na_5SmSi_4O_{12}$	22.164 (4)	12.661 (4)	5386
$Na_5ScGe_4O_{12}$	22.328 (2)	12.790 (2)	5522
$Na_5InGe_4O_{12}$	22.362 (1)	12.828 (1)	5555
$Na_5LuGe_4O_{12}$	22.583 (1)	12.899 (2)	5697
$Na_5YbGe_4O_{12}$	22.609 (2)	12.917 (2)	5718
$Na_5TmGe_4O_{12}$	22.634 (1)	12.924 (1)	5734
$Na_5ErGe_4O_{12}$	22.654 (2)	12.935 (2)	5749
$Na_5HoGe_4O_{12}$	22.683 (2)	12.949 (3)	5770
$Na_5YGe_4O_{12}$	22.697 (1)	12.958 (1)	5780
$Na_5DyGe_4O_{12}$	22.716 (3)	12.969 (3)	5795
$Na_5TbGe_4O_{12}$	22.737 (3)	12.973 (3)	5808
$Na_5GdGe_4O_{12}$	22.781 (1)	12.994 (2)	5840
$Ag_5GdSi_4O_{12}$	22.269 (2)	12.912 (1)	5545
$Ag_5YSi_4O_{12}$	22.175 (1)	12.859 (1)	5476

Table III. DTA Results on $Na_5MSi_4O_{12}$ Compositions

$Na_5FeSi_4O_{12}$	Heat: exotherm, 505 °C;[a] melt, 815 °C
	Cool: no thermal events
$Na_5ScSi_4O_{12}$	Heat: broad exo, 600 °C; endo, 810 °C; melt, 1200 °C
	Cool: exo, 1055 °C; 650 °C
$Na_5InSi_4O_{12}$	Heat: v broad exo, 660°; melting, 1100 °C
	Cool: exo, 610 °C
$Na_5LuSi_4O_{12}$	Heat: broad exo, 600 °C; endo, 800 °C; melting, 1215 °C
	Cool: exo, 595 °C
$Na_5ErSi_4O_{12}$	Heat: v broad exo, 600 °C; endo, 800 °C; melt, 1190 °C
	Cool: weak exo, 1070, 630 °C
$Na_5YSi_4O_{12}$	
(hydrothermal crystals)	Heat: melting, 1240 °C
	Cool: weak exo, 960, 630 °C
(powder)	Heat: endo, 790 °C; melt, 1225 °C
	Cool: exo, 615 °C
(powder)	Heat: endo, 810 °C; melt, 1200 °C
	Cool: exo, 660 °C
$Na_5GdSi_4O_{12}$	Heat: melt, 1120 °C
	Cool: exo, 1100 °C

[a] Temperature at which thermal event is initiated.

3.28, and 3.17 Å appears and is stable to 1025 °C. This phase is retained on quenching. Such behavior is incompatible with the fact that rhombohedral $Na_5ScSi_4O_{12}$ was prepared at 1100 °C and we conclude that the differences arise because the HT Guinier sample was heated under vacuum.

A similar HTG under vacuum was obtained for hydrothermally grown crystals of $Na_5YSi_4O_{12}$. At 600 °C a C_3A phase appears as in $Na_5ScSi_4O_{12}$. There is no corresponding DTA peak. By 800 °C $Na_5YSi_4O_{12}$ (NYS) disappears. At 985 °C the C_3A phase transforms to an unidentified phase with strong lines at 4.1, 3.45, and 3.15 Å which is stable on quenching. When the HTG was repeated in air with another sample of $Na_5YSi_4O_{12}$ prepared by solid-state reaction, the NYS structure was retained until 700 °C. Between 700 and 800 °C, transition to the C_3A phase begins and is complete at 850 °C. This phase is stable to 975 °C and does not revert to NYS after cooling to room temperature in 20 h. Apparently, the DTA endotherm at ~800 °C represents this NYS–C_3A transition, but again this is incompatible with preparation of NYS at 1000 °C. Perhaps heating conditions in the HT Guinier camera (a thin layer of finely divided sample on a Au support) favor this transition. A HTG run on $Na_5SmSi_4O_{12}$ under vacuum resulted in similar behavior. The C_3A phase appears at 640 °C and is stable up to 900 °C. At 950 °C an unidentified phase with strong lines at 4.1, 3.5, and 3.2 Å appears. The composition $Na_{4.9}Gd_{0.9}Zr_{0.1}Si_4O_{12}$ behaved somewhat differently from the other NYS compounds. A transition to the C_3A phase occurs at 940 °C.

HTG patterns of $Na_5SmSi_4O_{12}$ were taken between room temperature and 585 °C. Figure 1 shows plots of *a*, *c*, and *V* vs. temperature. Thermal expansion coefficients ($\alpha_T = (1/V)[(V_T - V_{20})/(T - 20)]$) were $\alpha(200\ °C) = 52 \times 10^{-6}\ (°C)^{-1}$, $\alpha(330\ °C) = 46 \times 10^{-6}\ (°C)^{-1}$, and $\alpha(470\ °C) = 43 \times 10^{-6}\ (°C)^{-1}$.

Powders of $Na_5YSi_4O_{12}$ and $Na_5GdSi_4O_{12}$ were treated with molten $LiNO_3$, $AgNO_3$, or KNO_3 at 300–350 °C for about 16 h and washed in warm H_2O in an attempt to make the corresponding Li^+, Ag^+, or K^+ compositions. The salt used was about 20 times that needed for complete ion exchange. The extent of exchange was determined by weighing the powders before and after treatment. The results, which ignore possible exchange with H_3O^+, are given in Table IV.

Refined lattice parameters for the Ag compounds are given in Table II. We were unable to determine the cell dimensions of the Li^+ compositions because the x-ray patterns were complex. Splitting of numerous lines in the powder patterns for the compositions $Na_{5-x}Li_xGdSi_4O_{12}$ ($x > 0.2$) prepared by solid-state reactions indicated some structural distortion.

Samples for conductivity measurements were prepared as either 0.5 or 0.25 in. diameter disks by pressing at 12000–100000 psi, heating in air for 4 h at 1000–1100 °C, and quenching in air. These were mounted in a stainless steel holder between two disks of 0.015 in. thick Na foil, supported on Ni screens. The temperature was raised above the melting point of Na metal to ensure good contact. Ac conductance

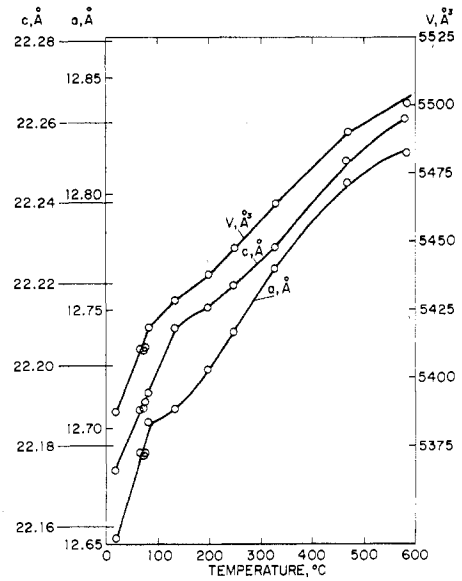

Figure 1. Cell dimensions of $Na_5SmSi_4O_{12}$ vs. T.

Table IV. Results of Ion Exchange Experiments

Ion exchange composition	Molten salt temp, °C	% exchange accomplished[a]
$Ag_5GdSi_4O_{12}$	300	91
$Li_5GdSi_4O_{12}$	300	86
$Li_{4.9}Gd_{0.9}Zr_{0.1}Si_4O_{12}$	350	14
$K_5GdSi_4O_{12}$	350	0
$Ag_5YSi_4O_{12}$	350	99
$Li_5YSi_4O_{12}$	350	100
$K_5YSi_4O_{12}$	350	0

[a] Based on weight change.

was measured from 280 to ~75 °C using a Wayne-Kerr universal bridge at a frequency of 1.6×10^3 Hz. Dc conductivity was measured by applying a slowly varying voltage (a triangular-wave form with a frequency less than 0.01 Hz) and recording the current. On removal, samples were checked for attack by Na. Most of the silicate compositions showed no Na attack. $Na_5SmSi_4O_{12}$ was an exception—the sample was gray in several areas, and Na globules were visible around the perimeter of the pellet. Reduction of Sm^{3+} to Sm^{2+} is consistent with the relative stabilities of the divalent and trivalent chlorides.[14] Most of the germanates were attacked. Some compositions such as $Na_5YGe_4O_{12}$, $Na_5ErGe_4O_{12}$, and $Na_5YbGe_4O_{12}$ showed partial or complete brown discoloration and a marked drop in conductivity on cooling at ~250 °C.

Most conductivity samples had densities ~70–90% of theoretical and therefore many conductivity values are probably low by factors of 2–5.[7] Electronic conductivity is believed to be negligible for these rare earth silicates.

Results and Discussion

Figure 2 shows good correspondence between r^3 and unit cell volumes except for $Na_5InSi_4O_{12}$ and $Na_5InGe_4O_{12}$. Such an anomaly was also noted for $NaInSi_2O_6$.[15] Because the Eu^{3+} compound was always contaminated with a $Ca_3Al_2O_6$-like phase similar to $Na_4CaSi_3O_9$[16] or $NaCa_{8.5}Al_6O_{18}$,[17,18] we did not list its cell dimensions or measure the conductivity. This C_3A type impurity phase that frequently accompanies $Na_5MSi_4O_{12}$ compounds can generally be eliminated only by repeated ball milling and reheating. Although its composition is not known, $Na_3MSi_3O_9$ compounds have a similar pattern. If $Na_3MSi_3O_9$ is present, Na_2SiO_3 must also be present to retain stoichiometry. However, since no diffraction lines from Na_2SiO_3 were observed, it must be assumed that Na_2SiO_3, if present, must be amorphous. Although unlikely because glassy Na_2SiO_3 is difficult to prepare,[19,20] it is conceivable that dispersion of Na_2SiO_3 at the grain boundaries may somehow

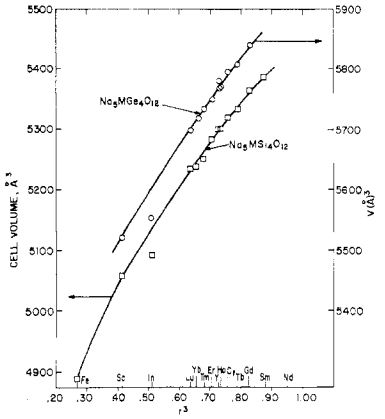

Figure 2. Cell volumes of $Na_5MSi_4O_{12}$ and $Na_5MGe_4O_{12}$ vs. r^3. Ionic radii are from ref 21.

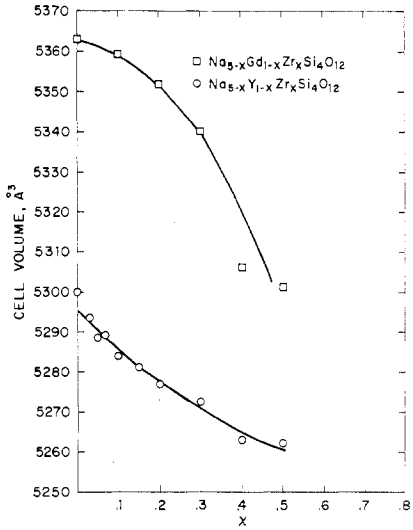

Figure 3. Cell volumes of $Na_5Gd_{1-x}Zr_xSi_4O_{12}$ and $Na_{5-x}Y_{1-x}Zr_xSi_4O_{12}$ vs. x.

favor formation of amorphous Na_2SiO_3. If amorphous Na_2SiO_3 is not present, then the composition of the C_3A-type phase must be different from $Na_3MSi_3O_9$.

The compounds $Na_5MSi_4O_{12}$ containing the larger rare earths Nd^{3+}, Pr^{3+}, and La^{3+} could not be prepared, but partial substitution for Gd or Sm was successful. The extent is determined largely by the $Na_5YSi_4O_{12}$ structure tolerances—the average ionic radius $\bar{r}$ must be kept below a limiting value of about 0.96 Å. Limiting values can be achieved, for example, by the combinations $Gd_{0.8}La_{0.2}$ ($\bar{r}$ = 0.956), $Gd_{0.6}Pr_{0.4}$ ($\bar{r}$ = 0.958), and $Gd_{0.4}Nd_{0.6}$ ($\bar{r}$ = 0.965),[21] corresponding to a maximum cell volume of ~5400 Å^3 for silicates and ~5840 Å^3 for germanates.

Zr and Hf may be substituted for Gd in $Na_{5-x}Gd_{1-x}Zr_xSi_4O_{12}$ up to $x \simeq 0.5$. Less Th may be substituted—x(Th) $\simeq$ 0.1. Figure 3 shows cell volume vs. composition for $Na_{5-x}Y_{1-x}Zr_xSi_4O_{12}$ and $Na_{5-x}Gd_{1-x}Zr_xSi_4O_{12}$. As expected Zr^{4+} substitution for M^{3+} causes a volume decrease in both cases, more rapidly for Gd^{3+} than Y^{3+}.

Complete solid solution between $Na_5GdSi_4O_{12}$ and $Na_5GdGe_4O_{12}$ exists. Although no others were attempted, solid solution probably exists where both end members are stable (see Table II). The range of stability of the germanates with respect to the size of the M^{3+} ions appears to be slightly smaller than that of the silicates.

Table V lists σ and E_a for various $Na_5MSi_4O_{12}$ phases and their solid solutions. Figure 4 shows log σ vs. $1/T$ plots for several of the $Na_5MSi_4O_{12}$ compounds. The largest rare earth ions give the highest conductivity.

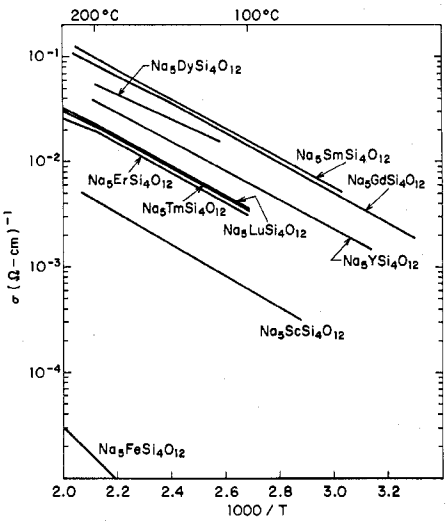

Figure 4. Log conductivity vs. $1/T$ for $Na_5MSi_4O_{12}$.

Values of σ and E_a are somewhat dependent upon the freedom from the C_3A impurity phase. Because a decrease in σ and a corresponding increase in E_a result from the presence of this phase, we assume it has a lower σ than the NYS-type phases. The conductivity of $Na_3GdSi_3O_9$, for example, is 2×10^{-5} $(\Omega\ cm)^{-1}$ at 300 °C. However, even when no impurities could be detected by x-ray analysis, small quantities (<2–5%) of this phase could not be excluded. This factor, in addition to the density problem, makes the values in Table V only approximate. The σ values listed are generally the highest observed. Because of better adaptability to practical uses (better resistance to Na attack than NSmS, and higher σ than NYS or NDyS) more effort was spent on $Na_5GdSi_4O_{12}$. Values listed for NGS are the average of five independent samples with E_a from 5.6 to 7.2 kcal/mol and A from 2 to 7×10^4 ($\sigma = A/T \exp(E_a/RT)$). The σ–$1/T$ plots frequently show a change in slope at 120–180 °C. We attribute this to a second phase of lower conductivity at the grain boundaries—perhaps the C_3A or an amorphous phase. E_a and A values listed in Table V were obtained primarily at ~200 °C.

The structure of $Na_5YSi_4O_{12}$[12,22] is characterized by SiO_4 tetrahedra linked to form puckered $Si_{12}O_{36}$ rings parallel to the basal plane of the hexagonal cell. These rings, separated by Na(2) tetrahedra and Na(3) octahedra are stacked to form large rigid columns parallel to c (see Figure 5). In the cores of the columns are three types of Na atoms: Na(2) in tetrahedral, Na(1) and Na(3) in octahedral sites. The columns are linked by YO_6 octahedra near the screw axes at $^1/_3$, 0 to form a three-dimensional framework with large channels between the rings (Figure 5a). The framework is exactly that proposed by Maksimov et al.[12] and accounts for 48 of the 90 Na atoms in the $Na_{90}Y_{18}Si_{72}O_{216}$ unit cell. These 48 Na atoms are tightly bonded in the columns and are probably immobile. The remaining 42 Na atoms, which Maksimov et al. failed to locate, were found in three independent sites, Na(4) near the screw axes similar to the Y atoms and Na(5) and Na(6) near the twofold axes at $^1/_2$, 0 (Figure 5b).[22] The difficulty in locating these Na atoms, the partial occupancy of these sites, and large apparent thermal parameters all imply that these Na atoms are highly mobile and the source of the high conductivity in NYS.

The YO_6 octahedra, which link the columns also hold them apart, leaving a large open channel near the twofold axes between two columns. Along these channels, Na atoms can move quite freely. These compounds should have excellent conductivity parallel to c and, therefore, might be expected to be highly anisotropic conductors. Although no conductivity

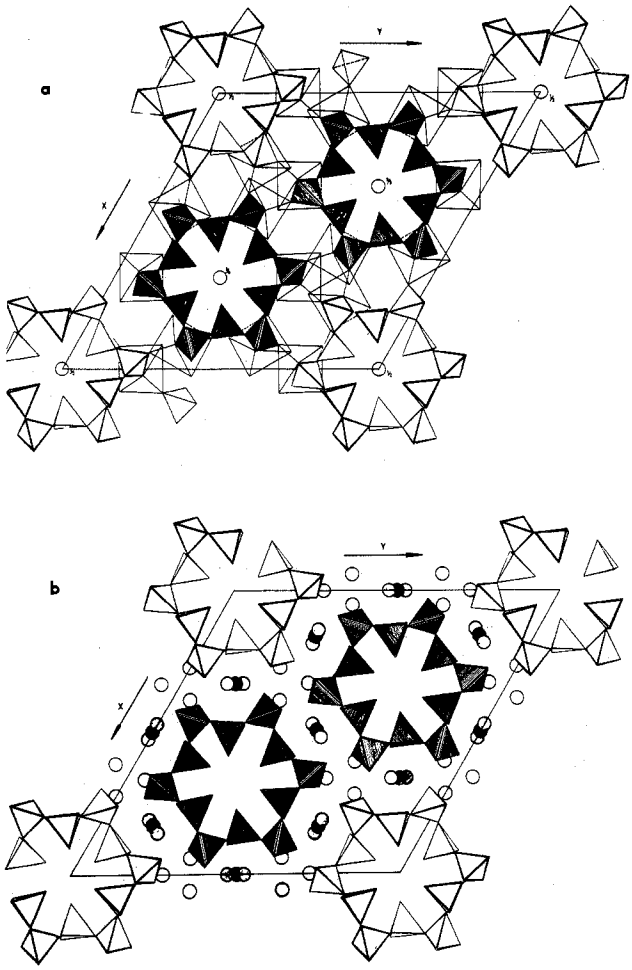

Figure 5. Projection of the $Na_5YSi_4O_{12}$ structure on (001). Part a shows location of $Si_{12}O_{36}$ rings and YO_6 octahedra: unshaded $Si_{12}O_{36}$ rings at $z \simeq 0$ and $^1/_2$; medium shaded $Si_{12}O_{36}$ rings at $z \simeq {}^1/_6$ and $^2/_3$; dark shaded $Si_{12}O_{36}$ rings at $z \simeq {}^1/_3$ and $^5/_6$; Y atoms in centers of octahedra. Part b shows location of mobile Na atoms: Na(4) unshaded circles at 18(e) (0.724, 0, 0.25); Na(5) black circles at 18(d) (0.5, 0, 0); Na(6) shaded circles at 36(f) (0.331, 0.144, 0.056).

measurements have been made on NYS single crystals, there appears, however, to be little similarity between the behavior of the NYS phases and known one-dimensional tunnel structures.[23,24] The apparent three-dimensional conductivity of NYS must arise from the presence of the Na(4) sites which serve as connecting links between the channels containing Na(5) and Na(6) sites. This conclusion is supported by the large apparent thermal motion of Na(4) in the direction of the two adjacent channels.

Because the $Si_{12}O_{36}$ rings are held apart by the MO_6 octahedra, the amount of "open" space between rings is determined largely by the size of the M^{3+} ion. This is clearly shown in Figure 2. Except for $Na_5InSi_4O_{12}$, there is almost a direct relationship between cell volume and ionic radius. Assuming that the critical channel size has not been reached, this should result in a continuous increase in conductivity with increase of the M^{3+} radius. There is in fact a good relationship between conductivities and ionic radii (Figure 6). The scatter in this figure probably can be attributed to variations in sample densities and C_3A impurity phases. Data from $Na_5FeSi_4O_{12}$ were omitted because of reaction with the Na electrodes. Samples containing mixed rare earths, such as $Na_5Gd_{0.8}La_{0.2}O_{12}$, $Na_5Gd_{0.6}Nd_{0.4}Si_4O_{12}$, and $Na_5Gd_{0.6}Pr_{0.4}Si_4O_{12}$, all have cell volumes larger than NGS. However, their conductivities are significantly lower (see Table V). This may be caused by impurities or the hexagonal NGS structure may be one where the optimum channel size is obtained with Gd.[25]

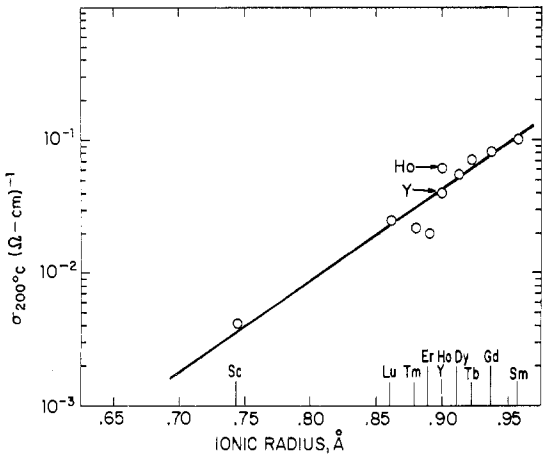

Figure 6. Conductivity of $Na_5MSi_4O_{12}$ vs. M^{3+} radius.

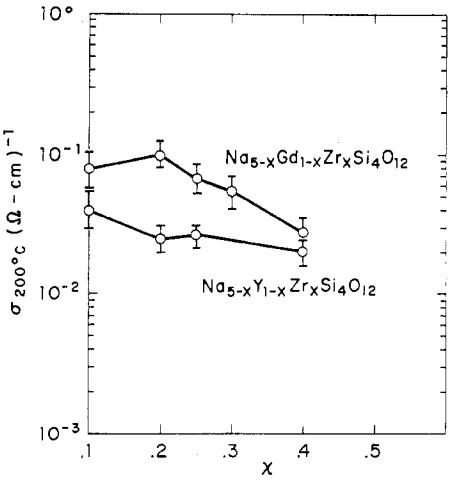

Figure 7. Conductivities of $Na_{5-x}Gd_{1-x}Zr_xSi_4O_{12}$ and $Na_{5-x}Y_{1-x}Zr_xSi_4O_{12}$ vs. x.

The conductivity variation with composition for $Na_{5-x}Gd_{1-x}Zr_xSi_4O_{12}$ and $Na_{5-x}Y_{1-x}Zr_xSi_4O_{12}$ is shown in Figure 7. In both solid solution series σ decreases as x increases, perhaps because of the decrease in cell volume and Na^+ concentration. $Na_{4.9}Gd_{0.9}Zr_{0.1}Si_4O_{12}$ appears to conduct slightly better than $Na_5GdSi_4O_{12}$, probably because of the improved sintering behavior of Zr-substituted compositions. $Na_{5-x}Gd_{1-x}Zr_xSi_4O_{12}$ pellets typically have fired densities greater than 95% of theoretical. ZrO_2 additions also seem to inhibit formation of the C_3A impurity.

In general, impurity phases reduce ionic conductivity. However, small quantities of Na_2SO_4 or Na_3PO_4 (1–2%) do not reduce σ significantly and indeed appear to improve sinterability. It may be that S^{6+} or P^{5+} enters the silicate framework, but sintering is probably enhanced by the presence of a liquid phase.

Additions of 0–20 mol % $Na_2Si_2O_5$ to conductive $Na_5MSi_4O_{12}$ phases do not significantly lower σ. Amorphous $Na_2Si_2O_5$ is known to be a Na^+ conductor with $\sigma = 5 \times 10^{-5}$ $(\Omega\ cm)^{-1}$ at 200 °C and 6.5×10^{-4} $(\Omega\ cm)^{-1}$ at 300 °C (Figure 8). Since $Na_2Si_2O_5$ forms a stable glass at 875 °C and is conductive, the retention of good conductivity could result from amorphous intergranular $Na_2Si_2O_5$. It may also react with $Na_5MSi_4O_{12}$ to form a nonstoichiometric phase.

Attempts to substitute Ba for Na in $Na_5YSi_4O_{12}$ or $Na_5GdSi_4O_{12}$ resulted in well-sintered multiphase products. The primary phase (80–100 mol %) is conductive $Na_5MSi_4O_{12}$, but an impurity phase (20 mol %) which may be a new composition $Na_3BaMSi_4O_{12}$ is also evident from the x-ray patterns. Because it is also conductive, relatively large amounts

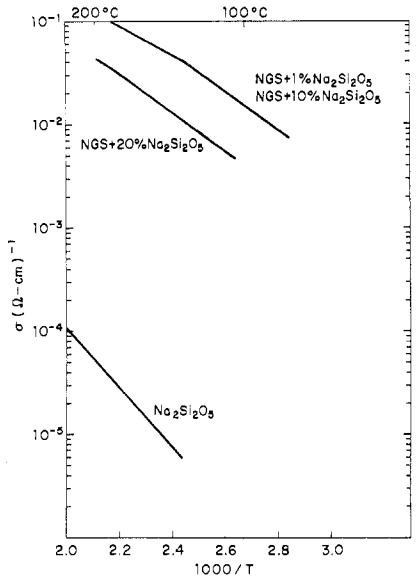

Figure 8. Conductivities of NGS–$Na_2Si_2O_5$ compositions vs. $1/T$.

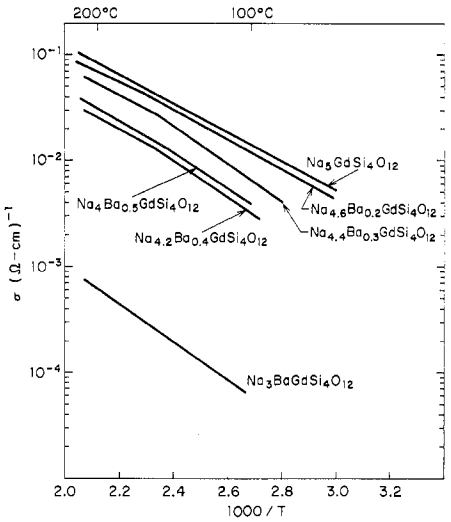

Figure 9. Conductivities of $Na_{5-2x}Ba_xGdSi_4O_{12}$ compositions vs. $1/T$.

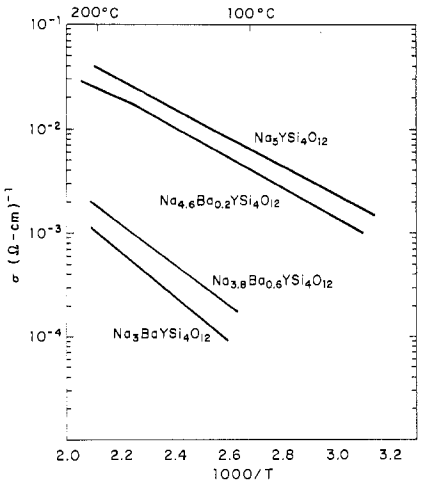

Figure 10. Conductivities of $Na_{5-2x}Ba_xYSi_4O_{12}$ compositions vs. $1/T$.

of this impurity do not significantly reduce σ. Figures 9 and 10 show that both $3Na_2O{\cdot}2BaO{\cdot}Gd_2O_3{\cdot}8SiO_2$ and $3Na_2O{\cdot}2BaO{\cdot}Y_2O_3{\cdot}8SiO_2$ have $\sigma \simeq 3 \times 10^{-3}$ $(\Omega\ cm)^{-1}$ at 300 °C.

The performance of NGS solid electrolytes was examined in a Na electrowinning cell and a Na–S cell. The elec-

Table V. Conductivity Data for $Na_5MSi_4O_{12}$ and $Na_5MGe_4O_{12}$ Phases

	% Theor. density	density g/cc	E_a kcal/mole	A*	Temperature range, °C	σ^{**}_{300} $(\Omega\text{-cm})^{-1}$	σ_{200} $(\Omega\text{-cm})^{-1}$
$Na_5FeSi_4O_{12}$	72	2.10	13.2	9×10^3	110-250	2×10^{-4}	2×10^{-5}
$Na_5ScSi_4O_{12}$	96	2.64	7 6	6×10^3	120-260	2×10^{-2}	4×10^{-3}
$Na_5LuSi_4O_{12}$	85	2.89	7.5	3×10^4	130-200	6×10^{-2}	2×10^{-2}
$Na_5YbSi_4O_{12}$	72	2.43	7.7	1×10^4	90-210	2×10^{-2}	8×10^{-3}
$Na_5TmSi_4O_{12}$	78	2.60	7.3	2×10^4	130-210	5×10^{-2}	2×10^{-2}
$Na_5ErSi_4O_{12}$	84	2.78	7.5	3×10^4	120-200	4×10^{-2}	2×10^{-2}
$Na_5YSi_4O_{12}$	81	2.31	7.1	3×10^4	100-180	1×10^{-1}	4×10^{-2}
$Na_5HoSi_4O_{12}$	91	3.00	7.4	6×10^4	100-230	2×10^{-1}	6×10^{-2}
$Na_5DySi_4O_{12}$	84	2.73	6.2	2×10^4	120-180	1×10^{-1}	6×10^{-2}
$Na_5TbSi_4O_{12}$	92	2.97	7.9	1×10^5	120-210	2×10^{-1}	7×10^{-2}
$Na_5GdSi_4O_{12}$	94	3.02	6.5‡	5×10^4‡	100-200	3×10^{-1}	8×10^{-2}
$Na_5SmSi_4O_{12}$	93	2.94	7.3	1×10^5	70-200	3×10^{-1}	1×10^{-1}
$Na_5Gd_{.8}La_{.2}Si_4O_{12}$	95	3.04	8.4	2×10^5	120-240	3×10^{-1}	5×10^{-2}
$Na_5Gd_{.6}Nd_{.4}Si_4O_{12}$	82	2.59	6.1	1×10^4	120-220	2×10^{-1}	5×10^{-2}
$Na_5Gd_{.6}Pr_{.4}Si_4O_{12}$	86	2.73	7.1	4×10^4	140-260	1×10^{-1}	4×10^{-2}
$Na_{4.9}Y_{.9}Zr_{.1}Si_4O_{12}$	74	2.13	6.2	9×10^3	100-200	7×10^{-2}	3×10^{-2}
$Na_{4.9}Y_{.9}Hf_{.1}Si_4O_{12}$	82	2.31	6.4	1×10^4	100-200	9×10^{-2}	3×10^{-2}
$Na_{4.9}Gd_{.9}Zr_{.1}Si_4O_{12}$	97	3.07	7.9	2×10^5	100-250	4×10^{-1}	1×10^{-1}
$Na_{4.9}Dy_{.9}Zr_{.1}Si_4O_{12}$	90	2.60	6.7	2×10^4	100-250	1×10^{-1}	4×10^{-2}
$Na_5TmGe_4O_{12}$	93	3.71	10.8	4×10^5	150-280	5×10^{-2}	7×10^{-3}
$Na_5HoGe_4O_{12}$	88	3.48	8.7	3×10^4	150-280	3×10^{-2}	7×10^{-3}
$Na_5DyGe_4O_{12}$	94	3.69	18.6	5×10^8	140-280	4×10^{-2}	3×10^{-3}
$Na_5TbGe_4O_{12}$	81	3.15	12.4	4×10^5	140-280	2×10^{-2}	2×10^{-3}
$Na_5GdSi_{3.75}Ge_{.25}O_{.2}$	93	3.04	7.3	8×10^4	90-230	3×10^{-1}	7×10^{-2}
$Na_5GdSi_3GeO_{12}$	94	3.19	6.5	3×10^4	140-240	1×10^{-1}	5×10^{-2}

*$\sigma = A/T \exp(-E_a/kT)$

**extrapolated value

‡average of six samples

trowinning cell, +|Na(Hg)/$Na_5GdSi_4O_{12}$/Na in Ni felt|−, was assembled in an Ar drybox. The cathode compartment was formed by sealing a disk of $Na_5GdSi_4O_{12}$ (2.21 cm in diameter and 0.183 cm thick) to the end of Pyrex glass tubing using Cotronics 940 ceramic cement. Ni felt inside the glass tubing in contact with the solid electrolyte served as the initial cathode contact. The anode consisted of 100.76 g of Na–Hg amalgam (0.46 g of Na). The cell was heated to 170 °C and connected to a Princeton Applied Research potentiostat (Model 173 with 179 digital coulometer) which served as the power supply. The electrolysis was performed at 2 V and the current density varied from 15 to 50 mA/cm^2. After 85% of the Na was removed from the amalgam (based on the amount of charge passed), the Na cathode deposit was dissolved in methanol and diluted with water and the resultant NaOH titrated with a standard HCl solution. The results showed that sodium had been transported with 99% current efficiency. Thus, the electronic conductivity is at least 2 orders of magnitude smaller than the ionic conductivity.

A sodium–sulfur cell, −|Na/$Na_{4.9}Gd_{0.9}Zr_{0.1}Si_4O_{12}$/$Na_2S_4$/graphite felt|+, was assembled in an Ar atmosphere from the following components: (1) an anode of Na (0.46 g); (2) a solid electrolyte disk (1.10 cm in diameter, 0.38 cm thick) sealed to the end of Pyrex glass tubing; (3) the cathode compartment being the Pyrex tubing containing Na_2S_4 (2.24 g) and a graphite felt current collector. The cell was heated to 325 °C where Na and Na_2S_4 are molten. The open circuit voltage was 2.0 V. Cell charge and discharge behavior was linear up to a current of 30 mA/cm^2 at a cell voltage of 2.13 V. No attempt was made to maximize the power output of the cell. The purpose was to demonstrate that these solid electrolytes can be used in Na–S energy storage cells.

Anisotropic conductivity of Na-β-Al_2O_3 has prompted a search for good Na conductivity in framework or tunnel

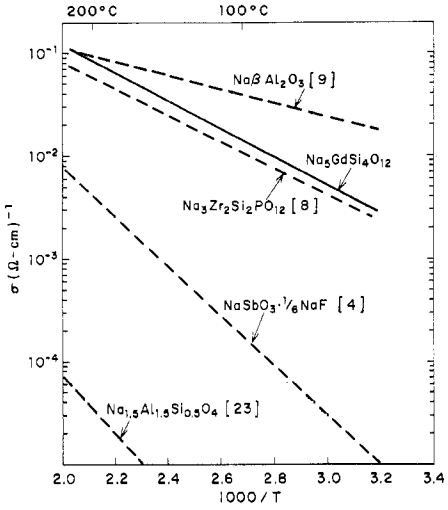

Figure 11. σ–$1/T$ plots for Na-conducting framework structures.

structures where three-dimensional conductivity might be expected. Good Na^+ mobility had been found previously in several framework structures—$Na_3Zr_2Si_2PO_{12}$,[8] $NaSbO_3$,[8,26] $NaTaWO_6$ (pyrochlore),[4] and $NaAlSiO_4$ (carnegieite).[8,27] The discovery of high ionic conductivity in NYS-type structures adds another structure type to this growing list. Figure 11 shows σ–$1/T$ plots for a number of these oxides having framework structures. There is an obvious increase in E_a in the series Na-β-Al_2O_3 (3.8 kcal/mol) < NGS (6 kcal/mol) < $NaSbO_3$ (10 kcal/mol) < $NaAlSiO_4$ (13 kcal/mol). NGS and $Na_3Zr_2Si_2PO_{12}$ have similar σ and E_a. At 25 °C Na-β-Al_2O_3 has the highest σ, but at about 200 °C, the two silicates and β-Al_2O_3 are approximately equivalent. The σ of $NaAlSiO_4$ is too low to be practical and $NaSbO_3$ and $NaTaWO_6$ are of doubtful stability in the presence of molten Na. Thus, the only promising materials of this group as practical solid electrolytes for use in high-temperature batteries are Na-β-Al_2O_3, $Na_5GdSi_4O_{12}$, and $Na_3Zr_2Si_2PO_{12}$. Although raw materials for both NGS and $Na_3Zr_2Si_2PO_{12}$ will be more costly than those of Na-β-Al_2O_3, they can be processed at lower temperatures. Both NGS and $Na_3Zr_2Si_2PO_{12}$ have potential only if pure dense ceramics can be fabricated, but this will probably require efforts similar to that expended on Na-β-Al_2O_3.

Acknowledgment. We would like to thank J. F. Whitney, G. A. Jones, and C. M. Foris for assistance in obtaining x-ray data, J. R. Barkley, T. S. Winant, and N. S. Ayares for making the conductivity measurements, and R. J. Bouchard and J. R. Barkley for critically reviewing the paper.

Registry No. $Na_5FeSi_4O_{12}$, 64362-54-5; $Na_5ScSi_4O_{12}$, 23425-05-0; $Na_5InSi_4O_{12}$, 65545-61-1; $Na_5LuSi_4O_{12}$, 65545-62-2; $Na_5YbSi_4O_{12}$, 65545-63-3; $Na_5TmSi_4O_{12}$, 65545-64-4; $Na_5ErSi_4O_{12}$, 65545-65-5; $Na_5HoSi_4O_{12}$, 65545-66-6; $Na_5YSi_4O_{12}$, 23425-16-3; $Na_5DySi_4O_{12}$, 65545-67-7; $Na_5TbSi_4O_{12}$, 65545-68-8; $Na_5GdSi_4O_{12}$, 64890-77-3; $Na_5SmSi_4O_{12}$, 65545-69-9; $Na_5ScGe_4O_{12}$, 65605-13-2; $Na_5InGe_4O_{12}$, 65605-12-1; $Na_5LuGe_4O_{12}$, 65605-11-0; $Na_5YbGe_4O_{12}$, 65605-10-9; $Na_5TmGe_4O_{12}$, 65605-09-6; $Na_5ErGe_4O_{12}$, 65605-08-5; $Na_5HoGe_4O_{12}$, 65605-07-4; $Na_5YGe_4O_{12}$, 65605-06-3; $Na_5DyGe_4O_{12}$, 65605-05-2; $Na_5TbGe_4O_{12}$, 65605-04-1; $Na_5GdGe_4O_{12}$, 65605-03-0; $Ag_5GdSi_4O_{12}$, 65545-70-2; $Ag_5YSi_4O_{12}$, 65545-71-3; $Li_5GdSi_4O_{12}$, 65545-72-4; $K_5GdSi_4O_{12}$, 65605-27-8; $Li_5YSi_4O_{12}$, 65605-28-9; $K_5YSi_4O_{12}$, 65605-29-0; $Na_5GdSi_3GeO_{12}$, 65605-30-3; $Na_3BaGdSi_4O_{12}$, 65545-73-5; $Na_3BaYSi_4O_{12}$, 65545-74-6; $Na_2Si_2O_5$, 13870-28-5; $Na_5LaSi_4O_{12}$, 65545-52-0; $Na_5NdSi_4O_{12}$, 65545-53-1; $Na_5PrSi_4O_{12}$, 65605-31-4; $Na_4ZrSi_4O_{12}$, 65545-54-2; $Na_4HfSi_4O_{12}$, 65545-55-3.

References and Notes

(1) J. B. Goodenough, J. Kafalas, and H. Y.-P. Hong, NASA Contract C-43205-C, Final Report Cr-134836 (March 1975).
(2) R. S. Roth, W. S. Brower, H. S. Parker, D. B. Minor, and J. L. Waring, NASA Contract C-50821-C, Final Report Cr-134869 (July 1975). NBSIR 75-754.
(3) W. L. Roth and O. Muller, General Electric Co. Technical Report SRD-74-034, NASA Cr-134610 (April 1974).
(4) J. Singer, W. L. Fielder, H. E. Kautz, and J. S. Fordyce, *J. Electrochem. Soc.*, **123**, 614 (1976).
(5) T. Takahashi in "Superionic Conductors", G. D. Mahan and W. L. Roth, Ed., Plenum Press, New York, N.Y., 1976, pp 379–394.
(6) B. A. Boukamp, I. D. Raistrick, C. Ho, Y.-W. Hu, and R. A. Huggins, ref 5, p 417.
(7) R. D. Shannon, B. E. Taylor, A. D. English, and T. Berzins, *Electrochim. Acta*, **22**, 783 (1977).
(8) J. B. Goodenough, H. Y.-P. Hong, and J. A. Kafalas, *Mater. Res. Bull.*, **11**, 203 (1976).
(9) M. S. Whittingham and R. A. Huggins, *Natl. Bur. Stand. (U.S.), Spec. Publ.*, **No. 364**, 139 (1972).
(10) N. L. Bowen, J. F. Schairer, and H. W. V. Willems, *Am. J. Sci.*, **20**, 405 (1930).
(11) B. A. Maksimov, B. N. Litvin, V. V. Ilyukhin, and N. V. Belov, *Sov. Phys.-Crystallogr. (Engl. Trans.)*, **14**, 407 (1969).
(12) B. A. Maksimov, Y. A. Kharitonov, and N. V. Belov, *Sov. Phys.-Dokl. (Engl. Transl.)*, **18**, 763 (1974).
(13) B. A. Maksimov, L. N. Dem'yanets, V. V. Ilyukhin, and Y. A. Kharitonov, *Acta Crystallogr., Sect. A*, **31**, S76 (1975).
(14) J. D. Corbett, D. L. Pollard, and J. E. Mee, *Inorg. Chem.*, **5**, 761 (1966).
(15) C. T. Prewitt, R. D. Shannon, and W. B. White, *Contrib. Mineral. Petrol.*, **35**, 77 (1972).
(16) I. Maki and T. Sugimura, *Yogyo Kyokai Shi.*, **78**, 129 (1970).
(17) F. Nishi and Y. Takeuchi, *Acta Crystallogr., Sect. B*, **31**, 1169 (1975).
(18) M. Regourd, S. Chromy, L. Hjorth, H. Hornain, and B. Mortureux, *Rev. Mater. Constr. Trav. Publics*, **No. 682**, 7 (1973).
(19) D. Ravaine, Thesis, University of Grenoble, 1976.
(20) A. C. J. Havermans, N. H. Stein and J. M. Stevels, *J. Non-Cryst. Solids*, **5**, 66 (1970).
(21) R. D. Shannon, *Acta Crystallogr., Sect. A*, **32**, 751 (1976).
(22) H.-Y. Chen, W. Jeitschko, T. E. Gier and R. D. Shannon, to be submitted for publication.
(23) J. Singer, H. E. Kautz, W. L. Fielder, and J. J. Fordyce in "Fast Ion Transport in Solids, Solid State Batteries and Devices", W. van Gool, Ed., North-Holland, Amsterdam, 1973, pp 653–663.
(24) H. U. Beyeler, T. Hibma and C. Schuler in "Superionic Conductors", G. D. Mahan and W. L. Roth, Ed., Plenum Press, New York, N.Y., 1976, pp 425–426.
(25) W. H. Flygare and R. A. Huggins, *J. Phys. Chem. Solids*, **34**, 1199 (1973).
(26) J. L. Waring, R. S. Roth, H. S. Parker, and W. S. Brower, *J. Res. Natl. Bur. Stand., Sect. A*, **80**, 761 (1976).
(27) R. D. Shannon, unpublished data.